



## **Relativistic nucleon and electron production in the 2003 October 28 solar event**

L. I. Miroshnichenko, Karl-Ludwig Klein, Gérard Trottet, Pierre Lantos, E. V.  
Vashenyuk, Yu. V. Balabin, B. B. Gvozdevsky

### **► To cite this version:**

L. I. Miroshnichenko, Karl-Ludwig Klein, Gérard Trottet, Pierre Lantos, E. V. Vashenyuk, et al.. Relativistic nucleon and electron production in the 2003 October 28 solar event. *Journal of Geophysical Research Space Physics*, 2005, 110, <10.1029/2004JA010936>. <hal-03785636>

**HAL Id: hal-03785636**

**<https://hal.science/hal-03785636v1>**

Submitted on 25 Sep 2022

**HAL** is a multi-disciplinary open access archive for the deposit and dissemination of scientific research documents, whether they are published or not. The documents may come from teaching and research institutions in France or abroad, or from public or private research centers.

L'archive ouverte pluridisciplinaire **HAL**, est destinée au dépôt et à la diffusion de documents scientifiques de niveau recherche, publiés ou non, émanant des établissements d'enseignement et de recherche français ou étrangers, des laboratoires publics ou privés.



Copyright - All rights reserved

## Relativistic nucleon and electron production in the 2003 October 28 solar event

L. I. Miroshnichenko

Pushkov Institute of Terrestrial Magnetism, Ionosphere, and Radio Wave Propagation, Troitsk, Russia

K.-L. Klein, G. Trottet, and P. Lantos

Observatoire de Paris, Laboratoire d'Etudes Spatiales et d'Instrumentation en Astrophysique, Meudon, France

E. V. Vashenyuk, Y. V. Balabin, and B. B. Gvozdevsky

Polar Geophysical Institute, Apatity, Russia

Received 30 November 2004; revised 4 June 2005; accepted 15 June 2005; published 30 September 2005.

[1] A flare on 2003 October 28 produced a relativistic particle event at Earth, although the active region AR 10486 was located to the east of the central meridian of the Sun. The paper considers features related to the acceleration at the Sun and the propagation to the Earth of energetic particles in this event, which occurred on a disturbed interplanetary background caused by preceding activity on the Sun and a corotating high-speed solar wind stream. From a study of the onset times of the event at different neutron monitors, we conclude that the earliest arriving solar particles were neutrons. The first relativistic protons arrived a few minutes later. Among relativistic solar protons (RSP), two populations could clearly be distinguished: prompt and delayed ones. The prompt solar protons caused an impulse-like increase at a few neutron monitor stations. The delayed solar protons arrived at Earth 0.5 hours later. Both prompt and delayed relativistic protons arrived at Earth from the antisunward direction. On the other hand, subrelativistic electrons that were traced by their radio emission from meter waves (Nançay Radioheliograph and Decametric Array) to kilometer waves (Wind/WAVES) are accompanied by metric radio emission in the western solar hemisphere, far from the flaring active region. We propose a scenario that reconciles the unusual features of energetic particles at the Earth with the observed structure of the interplanetary magnetic field, which suggests the Earth is at the interface between an interplanetary coronal mass ejection (ICME) and a corotating stream during the event. In this scenario the high-energy protons and electrons are accelerated in the flaring active region, injected into the eastern leg of an ICME loop rooted in the active region, and reach the Earth from the antisunward direction after passing through the summit of the loop. We attribute the promptly escaping subrelativistic electrons to acceleration in the western solar hemisphere and propagation along the nominal Parker spiral.

**Citation:** Miroshnichenko, L. I., K.-L. Klein, G. Trottet, P. Lantos, E. V. Vashenyuk, Y. V. Balabin, and B. B. Gvozdevsky (2005), Relativistic nucleon and electron production in the 2003 October 28 solar event, *J. Geophys. Res.*, **110**, A09S08, doi:10.1029/2004JA010936.

### 1. Introduction

[2] Relativistic solar energetic particle events (ground-level enhancements (GLEs)) usually accompany flares located in the western hemisphere, near the footpoint of the nominal Parker spiral connected with the Earth. However, in a few cases, GLEs were found with flares in the eastern hemisphere. They have been attributed to protons resulting from the decay of primary neutrons on the nominal interplanetary field line [Evenson *et al.*, 1983; Shea *et al.*, 1991]

or to acceleration sites far from the flaring active region [Klein *et al.*, 1999, 2001]. Acceleration on the well-connected field line by an extended coronal shock wave [Lockwood *et al.*, 1990] is a further possibility. Some authors consider the idea that prompt particle enhancements in some eastern events can be due to connection to the Earth by means of the field lines of an earlier coronal mass ejection (CME) [Richardson *et al.*, 1991, 1996; Kahler and Reames, 1991]. The particle event of 28 October 2003 is another GLE related to a nominally not well-connected flare. In this paper we study the radio emission in a wide diapason including metric-to-kilometric radio emission from electrons accelerated during the early rise

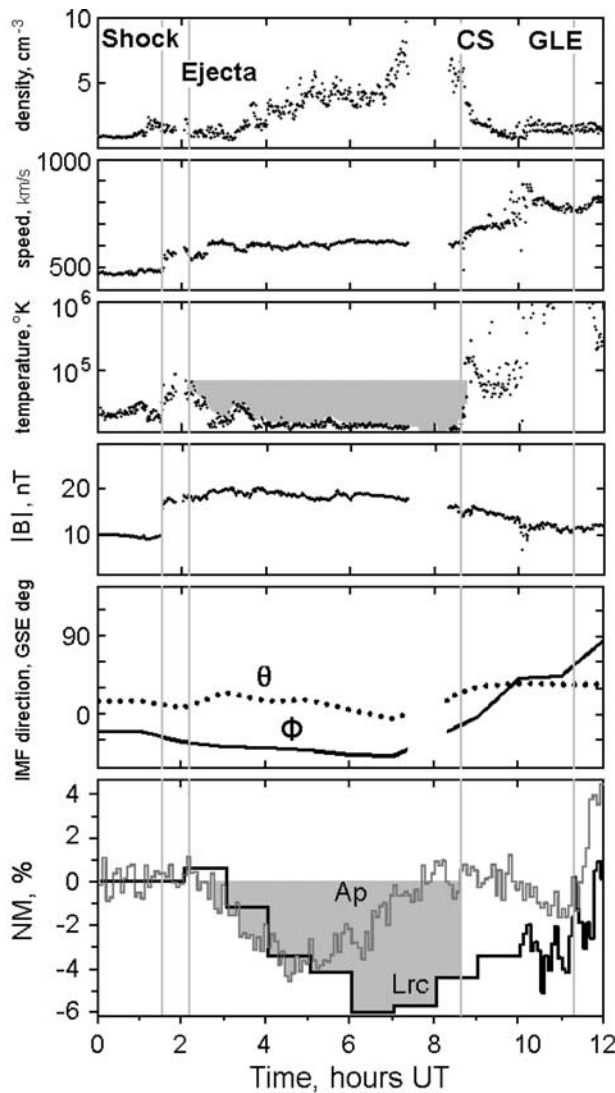


**Figure 1.** A plot of solar wind and interplanetary magnetic field parameters for 28 October 2003 (top to bottom) the proton density, the bulk velocity, the temperature, the magnetic field strength, the elevation ( $\theta$ ) and azimuth ( $\Phi$ ) of the magnetic field direction in solar ecliptic coordinates, cosmic ray intensity variations: neutron monitors Apatity (Ap) and LARC (Lrc). Vertical lines show the times of a shock, border between ejecta and corotating stream (CS) of a fast solar wind, and ground-level enhancement (GLE) onset. The darkened area is a low temperature and cosmic ray depression region, indicative of ejecta.

of the neutron monitor signals in an attempt to understand the acceleration and propagation of charged energetic particles during the event and their propagation to Earth. The energetic spectra and also directional characteristics of relativistic solar protons derived from the data of neutron monitors can reveal possible sources of the accelerated particles on the Sun. On the basis of the obtained data on solar radio emission and characteristics of energetic particles the features of generation and propagation to the Earth of particles of various species and energies are studied. A preliminary account of the neutron monitor and radio data

was given by Miroshnichenko *et al.* [2005], but we come to a different conclusion on the origin of the relativistic protons in the present paper.

## 2. General Characteristics of the Event

[3] The GLE on 28 October 2003 accompanied a large flare (4B, X17.2) that occurred in the active region NOAA 10486 slightly east of the central meridian (S16, E08), together with smaller flares in neighboring active regions (S06 E02, N09 E02; San Vito Observatory, in solar geophysical data). The H-alpha patrol at Meudon Observatory (<http://bass2000.obspm.fr>) noted the first signature of the flare in the red wing of the line shortly before 1000 UT. At 1102 UT bright ribbons appeared. They spread apart and faded away after 1200 UT. During this time a filament was observed to move rapidly toward northwest, reaching well into the western solar hemisphere. The EIT instrument aboard SOHO (195 Å) observed bright narrow emission features along the path of this filament in the images of 1124, 1136, and 1148 UT [Delaboudinière *et al.*, 1995]. The SOHO/LASCO coronagraph saw a halo CME with speed  $\sim 2500$  km/s since 1130 UT [Yashiro *et al.*, 2004] (CME catalogue, [http://cdaw.gsfc.nasa.gov/CME\\_list](http://cdaw.gsfc.nasa.gov/CME_list)).

[4] The event on 28 October 2003 occurred on a background of interplanetary disturbance connected to passage through the Earth of an interplanetary CME (ICME), ejected from the Sun on 26 October during a 3B/X1.2 flare 15S 44E occurred at 0617 UT in the active region AR10486 [Veselovsky *et al.*, 2004; Ivanov *et al.*, 2005]. It is necessary to note that later on that day one more flare 2N/X1.2 (2126 UT) has occurred but in AR10484 (01N 38W). The event was related with a full halo CME and was a source of a moderate SPE. Both events were comparable in strength and occurred symmetrically in respect to the central meridian. However, the source of a shock (0131 UT), Forbush effect, and interplanetary disturbance early on 28 October was the flare in the AR10486 as Ivanov *et al.* [2005] and Veselovsky *et al.* [2004] pointed out. Their analysis was based on comparison of the observable IMF characteristics with coronal sources.

[5] Figure 1 shows parameters measured on the ACE spacecraft of the solar wind (ACE/SWEPAM; <http://helios.gsfc.nasa.gov/ace/swepam.html>) and the interplanetary magnetic field (IMF) (ACE/MAG; <http://www.sec.noaa.gov/ace/>). At 0131 UT on 28 October, a shock reached ACE. After an initial increase the solar wind temperature dropped, which usually is an attribute of ejecta [Richardson and Cane, 1996; Cane, 2000]. Independent evidence that the Earth was within ejecta were the increase of the magnetic field strength  $B$ , and also a moderate amplitude Forbush-effect, which can be traced on the data of neutron monitors at Apatity and LARC (Antarctica, S62, E301). Owing to strong anisotropy of a Forbush-effect [Cane, 2000] the data of two neutron monitors looking in different directions are given in Figure 1.

[6] The direction of the IMF, measured by the azimuth  $\Phi$  (counterclockwise from the sunward direction in the ecliptic plane) and elevation  $\Theta$  (above the ecliptic plane) was close to the nominal Archimedian spiral ( $\Phi = -45^\circ$ ,  $\Theta = 0^\circ$ ) up to the minimum of the Forbush effect at about 0700 UT. Then, shortly before the GLE onset, the magnetic field turned

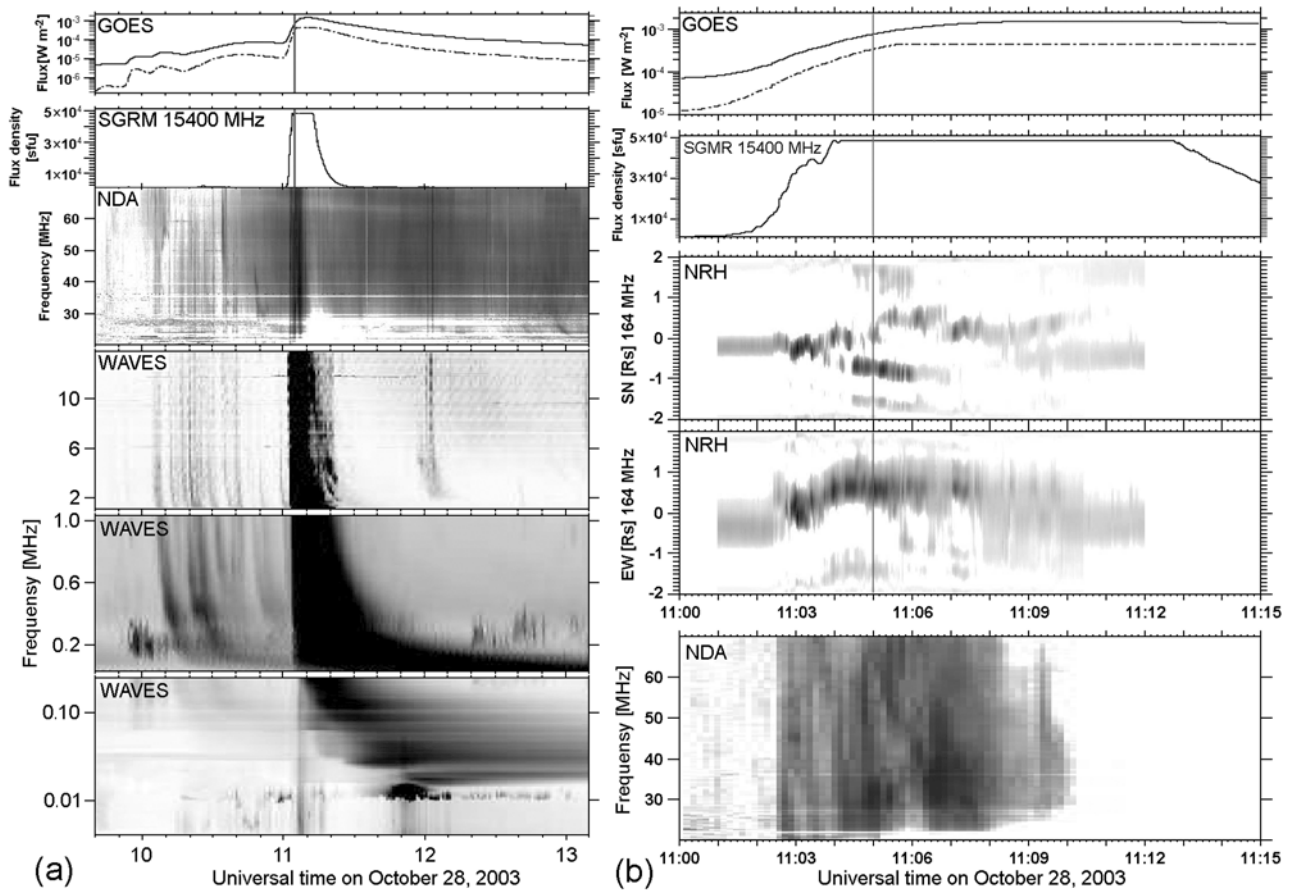


**Figure 2.** (a) Time history of electromagnetic emissions during the 28 October 2003 event. From top to bottom: soft X-ray flux (GOES), microwave flux (Sagamore Hill; saturated during part of the event), radio spectrum from long meter waves (Nancay Decametric Array) to kilometer waves (Wind/WAVES; black shading means high flux density). The vertical line in the two top panels mark the onset time of the neutron event on the Tsumeb neutron monitor (see Figure 4). (b) Time history of electromagnetic emissions during the brightest part of the 28 October 2003 event. From top to bottom: soft X-ray, microwave flux density, radio brightness at 164 MHz projected onto the solar south-north and east-west direction, respectively (Nancay Radioheliograph), spectrum at long meter wavelengths (after subtraction of the initial continuum emission). The vertical line in the four top panels gives the onset time of the event at the Tsumeb neutron monitor.

eastward by 90 degrees. Thus during the basic part of the GLE the direction of the IMF differed strongly from the nominal Archimedian spiral. That was a key to the unusual features of the 28 October 2003 event discussed below. At the same time, the east-west direction of the IMF is characteristic of ejecta near the orbit of the Earth [Richardson and Cane, 1996; Cane, 2000]. After about 0800 UT, temperature and speed of the solar wind increased with a simultaneous drop of density that signaled the entry of the Earth into a corotating high-velocity solar wind stream [Ivanov *et al.*, 2005]. This stream seems to originate from a coronal hole northwest of the AR 10486 (<http://spaceweather.com/index.cgi>). The coronal hole is seen in the northwestern quadrant of the Sun in the EIT 19.5 nm images in Figure 3. At the same time, the Forbush effect was in progress up to GLE onset (Figure 1), and we believe that at the beginning of the GLE the Earth was in a boundary area between the ejecta and the corotating stream.

[7] The solar wind speed then reached a value of about 760 km/s [Ogilvie *et al.*, 1995; Skoug *et al.*, 2004] (Wind/SWE, <http://web.mit.edu/afs/athena/org/s/space/www/wind.html>). The Parker spiral corresponding to the quoted speed is rooted near W30° and has a length of 1.04 AU. Recent analyses suggest [Veselovsky *et al.*, 2004; Skoug *et al.*, 2004] that after 1240 UT the solar wind ACE and Wind readings were unreliable due to detrimental effects of energetic solar protons.

### 3. Radio Observations

[8] Figure 2a shows the time history of electromagnetic radiation from the heated coronal plasma (soft X-rays, top, provided by the Solar Data Analysis Center at NASA Goddard Space Flight Center, <http://umbra.nascom.nasa.gov/>), from mildly relativistic electrons in the low corona (15.4 GHz microwaves, second from top; <http://www.ngdc.noaa.gov/stp/SOLAR/ftpsolarradio.html>) and



from nonthermal electrons from the high corona (long meter waves 20–70 MHz; third from top; Nançay Decametric Array) [Lecacheux, 2000] to 1 AU (14 MHz to 4 kHz spectrum from Wind/WAVES, <http://lep694.gsfc.nasa.gov/waves/waves.html>) [Bougeret et al., 1995]. At frequencies below 14 MHz (three bottom panels) a series of type III bursts is seen between 1000 and 1100 UT, followed by a much brighter type III burst which starts at frequencies above 70 MHz (NDA spectrum) and coincides with the rise of the brightest soft X-ray and microwave emission. The dynamic spectrum in the bottom panel of Figure 2a shows bright short-lasting and narrow-banded emissions shortly before 1200 UT, when the bright type III burst approaches the plasma frequency at the Wind spacecraft near 0.02 MHz. These emissions are Langmuir waves. They are generated locally by the type III emitting electron beams and demonstrate that the spacecraft intercepted the electron beams although the optical flare occurred in the eastern solar hemisphere. The spacecraft was hence magnetically connected with the acceleration region of these beams in the corona. From the time interval between the start of the type III emission at 70 MHz (1103 UT) and the start of the Langmuir waves at Wind (1143 UT), the exciter speed of the type III burst is about one fifth the speed of light ( $0.21c$  for a path length of 1.04 AU), corresponding to electrons of energy 11 keV, as is typical for interplanetary type III bursts.

[9] Hard X-ray and gamma-ray emission is observed by the CORONAS-F spacecraft [Kuznetsov et al., 2005; Veselovsky et al., 2004] and by the International Gamma Ray Astrophysics Laboratory (INTEGRAL) mission between 1102 and about 1110 UT [Gros et al., 2004]. These authors report evidence of electron acceleration up to several MeV and of different ion species. RHESSI missed the early part of the event but localized the hard X-ray sources in an arcade of flaring loops in AR 10486 (S. Krucker, personal communication, 2005). The same location is observed for the 210 GHz source produced by gyrosynchrotron emission from relativistic electrons [Lüthi et al., 2004]. The phase of bright radio emission shown in Figure 2a hence is the phase of most efficient acceleration of the interacting electrons and ions in the flaring active region.

[10] A zoom on the time interval around the bright decameter-to-hectometer wave (DH) type III bursts is shown in Figure 2b. The type III bursts are already visible, together with other intense emission including a type II burst and a broadband continuum, in the (20–70) MHz range (bottom panel of Figure 2b), which appears more pronounced than in Figure 2a because a preevent background was subtracted. The soft X-ray and microwave time histories of the full Sun emission are plotted in the two top panels. The third and fourth panel from the top show the evolution of the intensity and source position at 164 MHz observed by the Nançay Radioheliograph (NRH) [Kerdraon and Delouis, 1997]. The emission is plotted in projection onto the solar east-west (EW) and south-north (SN) directions. The uniform gray band before the bright DH type III bursts shows a noise storm south-east of disk center. In Figure 3 selected snapshot maps of the 164 MHz sources are overlaid as iso-intensity contours at half maximum on an EIT image at 19.5 nm taken shortly

before the flare. The noise storm (Figure 3a) projects to the eastern half of AR 10486, suggesting emission from high eastward extending loops. The emission reveals long-lasting electron acceleration in the active region, which is not directly related with the activity under discussion. Shortly after 1100 UT, at the start of the type III bursts at lower frequencies, the dominant 164 MHz source shifts to the western hemisphere and spreads more or less regularly toward both south and north at a projected speed  $\sim 1800 \text{ km s}^{-1}$  (Figure 2b). Figures 3b–3f show individual snapshots during this period, on top of the same EIT image. The presence of metric radio emission in the western solar hemisphere strongly suggests that electrons are accelerated there, far from the flaring active region. The southward and northward spread of the radio sources at a speed comparable with the halo CME suggests that the activation of remote acceleration sites is related to the CME development. At the end of the bright type III bursts the source switches back to the vicinity of AR 10486. Broadband decimetric-to-metric continuum (type IV) emission continues there during at least 4 hours, as documented by patrol observations (RSTN, Nançay), showing that electron acceleration continues in AR 10486 over a comparable duration. Multiple sources are observed at 164 MHz (Figures 3g–3i). They extend over the whole complex of active regions, including AR 10486 and its western and northwestern neighbors. The western radio sources in Figures 3g and 3i project above AR 10492 near  $30^\circ$  western longitude, which is close to the nominal connection length. It is thus not impossible that electrons accelerated after the phase of brightest radio emission continue to have direct access to the Earth along the nominal Parker spiral. In the higher-frequency band 270–25 MHz the intense group of type III radio bursts were observed by the radio spectrograph IZMIRAN (<http://helios.izmi-ran.troitsl.ru/lars/LARS.html>) during the time interval 1102–1110 UT [Veselovsky et al., 2004] (Figure 4).

#### 4. Relativistic Nucleon Observations: Evidence for Solar Neutrons

[11] The first solar energetic particles detected at Earth orbit were neutrons. Direct relativistic solar neutrons were registered by the neutron monitor at Tsumeb station (South Africa,  $S19.2^\circ$ ,  $E17.58^\circ$ , cutoff rigidity  $R_c = 9.21 \text{ GV}$ , altitude 1240 m above sea level). A small increase  $\sim 2\%$  in the 5-min data was observed between 1105 and 1115 UT [Miroshnichenko et al., 2004, 2005; Veselovsky et al., 2004; Bieber et al., 2005]. Figure 4 shows the data of neutron monitors at Tsumeb and Moscow. The arrow points to the onset of bright hard X-ray, gamma-ray, and radio emission at 1102 UT (section 3). Because of its high geomagnetic cutoff rigidity, the Tsumeb NM is likely unable to have registered protons from the Sun, while the stations with lower cutoffs did not see them at that time. The SONG instrument aboard the CORONAS-F space observatory (orbital altitude = 500 km, orbital inclination =  $82.5^\circ$ , and revolution period = 94.5 min) registered the direct solar neutrons in a time interval that nearly coincided with the excess at the Tsumeb neutron monitor [Kuznetsov et al., 2005]. During the start of the 28 October 2003 event the spacecraft was illuminated by the Sun, so the SONG instrument was capable of registering both the gamma

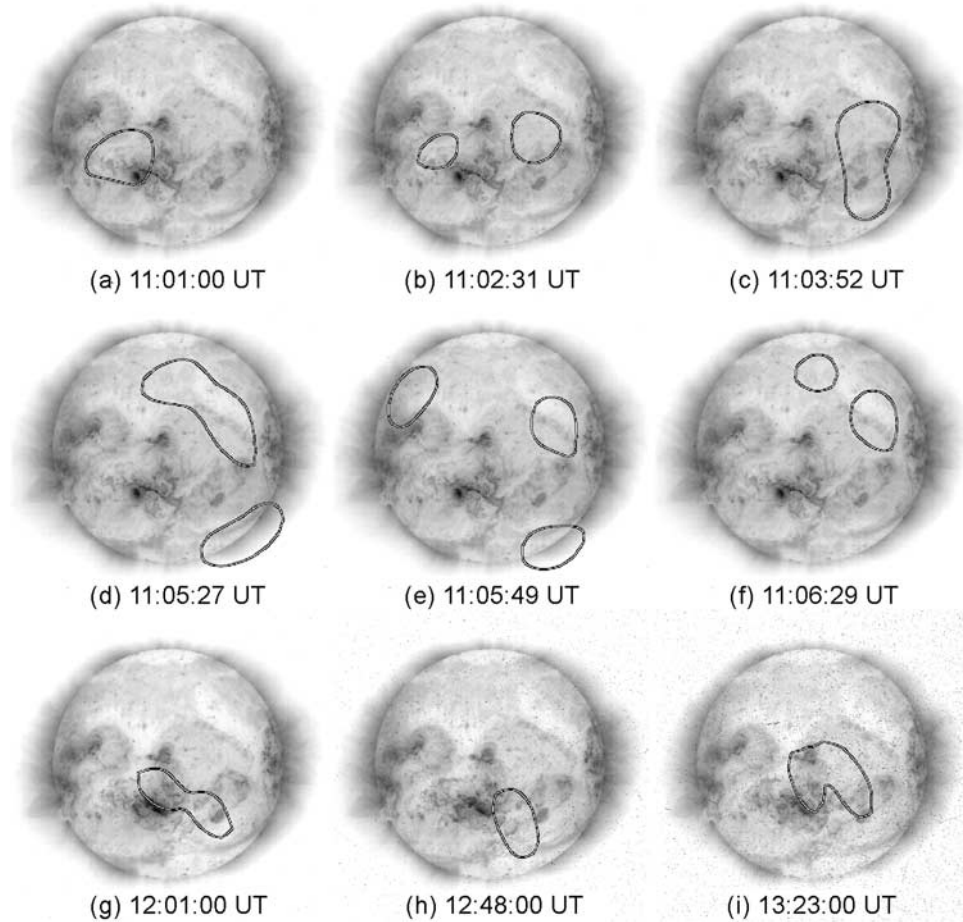


**Figure 3.** Snapshot maps at different times during the 28 October 2003 event at 164 MHz (contours at half brightness maximum; NRH) superposed on the EIT 195 Å image taken at 1100:10 UT, near the start of the flare (reverse color scale).

radiation and direct neutrons from the flare [Kuznetsov *et al.*, 2005]. Under the assumption that the first neutrons were emitted at the onset of the most conspicuous electromagnetic emissions from the corona (1102–1103 UT), the energy of the neutrons detected at Tsumeb is estimated to about 400–450 MeV from the delay of their arrival with respect to the electromagnetic radiation. The onset times derived from the increase profiles at different stations are listed in Table 1, together with the peak excess count rate (percentage of background) and with information on each station (location, cutoff rigidity, altitude above sea level, declination angle of the Sun at 1110 UT). We estimated the onset time as visual estimate of the time when the count rates definitely exceeded the background (column 7) declination angle. In our earlier paper [Miroshnichenko *et al.*, 2005], the onset time was estimated as a fit of the early rise by an exponential and evaluation of the intersection with the computed preevent background. As expected, the onset time from visual inspection (column 7) is in general close to the upper limit of the value derived from the exponential fit [Miroshnichenko *et al.*, 2005].

[12] At Tsumeb station the zenith distance of the Sun was about 79° during the flare. No other mountain neutron monitor registered this increase. Note, however, that the declination angle of the Sun at those stations were small, for

example, at Jungfraujoh station it was about 31.4° and at Yerevan it was about 26.3°. As a result, their sensitivity to primary neutrons was by more than an order of magnitude less in comparison with that for Tsumeb NM [Debrunner

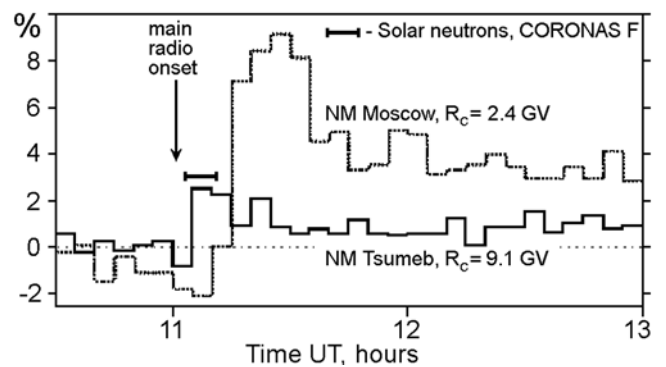


**Figure 4.** Increase profiles of the GLE observed with 5-min averages by Tsumeb and Moscow neutron monitors. The vertical arrow indicates the start of bright radio emission at 1102 UT. The horizontal bar marks the time when neutrons were detected by the SONG instrument at CORONAS-F spacecraft [Kuznetsov *et al.*, 2005].

**Table 1.** Onset Times of the GLE Measured By Different Neutron Monitors

Stations	Location	Altitude, m	$R_c$ , GV	Sun's Declination Angle	Peak Intensity, %	Onset Time, UT
Tsumeb	20S 18E	1240	9.21	79°	5	1105 ± 1
South Pole	90S 00E	2820	0.09	13°	18	1120 ± 1
McMurdo	80S 167E	48	0.00	2°	47	1118 ± 1
Norilsk	69N 88E	0	0.58	−9°	25	1112 ± 1
Moscow	57N 37E	200	2.40	17°	15	1114 ± 1
Terre Adelie	67S 140E	32	0.00	−3°	29	1112 ± 1

*et al.*, 1990]. Moreover, the simulations of *Stoker and Lemmer* [1992] demonstrate the high efficiency of the Tsumeb NM to the registration of solar neutrons. *Bieber et al.* [2005] reached the same conclusion and derived a duration of the injection of about 8 min, which is comparable to that of the electromagnetic emissions of electrons and ions during the flare.

[13] With the exception of the neutron monitor at Tsumeb (very weak signal) and the uncertain start at South Pole, the earliest onset time in Table 1 is 1112 ± 1 min UT. Since the Sun was below the horizon at Norilsk during the event, the rise at 1112 UT must be attributed to protons. Using a Parker spiral length of 1.04 AU and a propagation speed of the relativistic solar protons above 0.9 c (kinetic energy above 1 GeV), we infer that protons released onto the nominal interplanetary field line would need about 80 s more than the photons to reach the Earth. This would imply a solar release of relativistic protons not later than at 1110 UT − 8 min = 1102 UT. This is about 8 min after the onset of the most conspicuous electromagnetic emissions from the corona which one would usually consider as the most probable moment of relativistic SCR acceleration. It is also 8 min after the type III signature of electron acceleration in the western hemisphere (see section 3), emitting low-energy electrons on field lines that were connected with the Wind spacecraft. The delayed release of relativistic protons is thus difficult to reconcile with other data if the protons indeed propagate along the nominal Parker spiral. It is noteworthy that despite the delay, a relatively rapid rise, typical of well-connected events, was observed by neutron monitors for solar protons during this flare east of central meridian. This suggests to search for alternatives to the propagation along the nominal field line. Before addressing this issue, we consider the energy spectrum and pitch angle distribution of the relativistic protons.

## 5. Neutron Monitor Observations

[14] The GLE on 28 October 2003 was outstanding as it was observed at more than 30 neutron monitor stations of the worldwide network. In this section we will consider the behavior of relativistic solar protons (RSP) by their characteristics derived by modeling neutron monitor responses and fitting them to observations. So in section 5.1 the phenomenological picture of the GLE as it was observed at different neutron monitor stations is presented. Section 5.2 considers the neutron monitor response modeling technique and how the parameters of relativistic solar protons are obtained from observations by

the least squares procedure. In section 5.3 the dynamics of the derived RSP energy spectra and anisotropies is studied.

### 5.1. Neutron Monitor Network Data Processing and Modeling Technique

[15] With data of the worldwide neutron monitor network the parameters of RSP as well as their dynamics in the course of a given GLE can be obtained with the help of a modeling technique developed by *Shea and Smart* [1982], *Cramp et al.* [1997], and *Vashenyuk et al.* [2003a, 2003b]. Data from no less than 25–30 neutron monitor stations are required for such an analysis. Modeling process of the neutron monitor network response to an anisotropic RSP flux consists of several steps:

[16] 1. Determination of asymptotic viewing cones of the neutron monitor (NM) stations under study by the particle trajectory computations in a model magnetosphere.

[17] 2. Calculation of the NM responses as a function of solar proton flux parameters.

[18] 3. Determination by a least squares procedure (optimization) of the primary solar proton parameters outside the magnetosphere by comparison of computed neutron monitor responses with observations.

[19] Determination of asymptotic viewing cones of neutron monitor stations under study was carried out by computations of the particle trajectories in the magnetosphere model by *Tsyganenko-2001* [*Tsyganenko*, 2002a, 2002b] with a step in rigidity of 0.001 GV. The response function of a given neutron monitor to anisotropic flux of solar protons [*Shea and Smart*, 1982; *Cramp et al.*, 1997; *Vashenyuk et al.*, 2003b] is given by the relation

$$\left(\frac{\Delta N}{N}\right)_j = \sum_{R_c}^{20GV} J_{\parallel}(R) \cdot S(R) \cdot F(\theta_j(R)) \cdot A(R) \cdot dR, \quad (1)$$

where  $(\Delta N/N)_j$  is a percentage increase in the count rate  $N_j$  at a given NM station  $j$  and  $J_{\parallel}(R) = J_0 R^{-\gamma^*}$  corresponds to the rigidity spectrum of RSP flux  $J_{\parallel}(R)$  in the apparent source direction with changing slope (power law index  $\gamma^*$ ), and  $J_0$  is a normalization constant of the spectrum. In more detail, a change of spectral slope is described by the relation  $\gamma^* = \gamma + \Delta\gamma \cdot (R-1)$ , where  $\gamma$  is a power law spectral exponent at  $R = 1$  GV and  $\Delta\gamma$  is a rate of  $\gamma$  increase per 1 GV. The other parameters in (1) are  $S(R)$ , which is a specific yield function;  $\theta(R)$ , which is a pitch angle for a given particle (more precisely, an angle between the asymptotic direction at a given rigidity  $R$  and the anisotropy axis given by  $\Phi$  and  $\Lambda$ , the pairs of coordinates, longitude



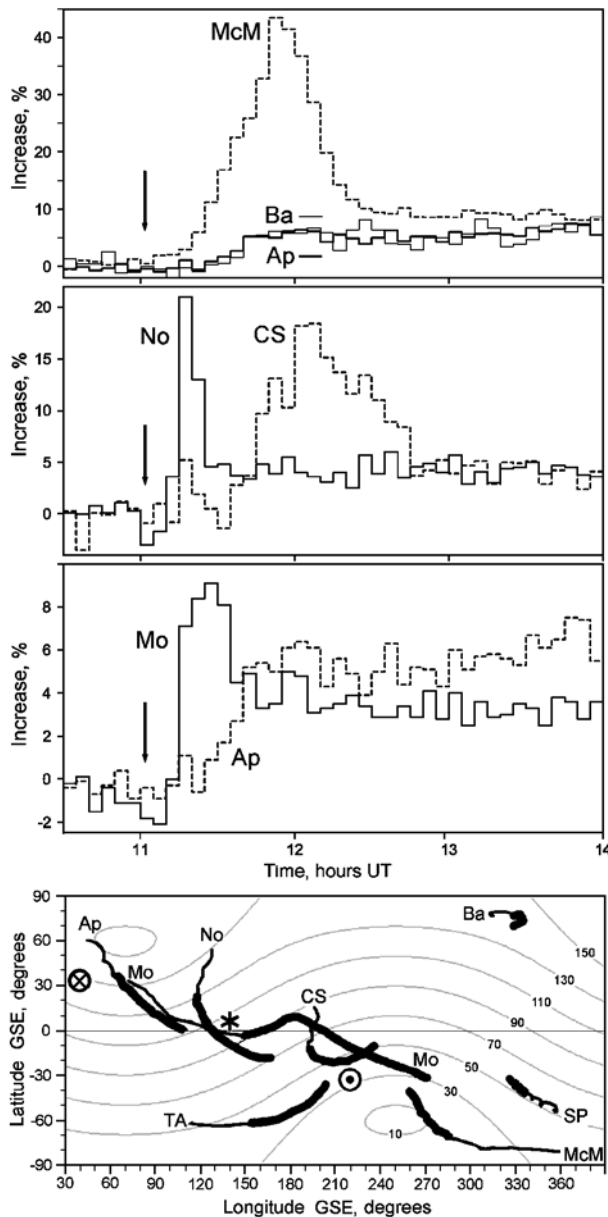


**Figure 5.** The event of 28 October 2003 in relativistic solar protons by the data of a number of neutron monitor stations: (a) AP-Apatity, BA-Barentsburg, McM-McMurdo; (b) NO-Norilsk, CS-Cape Schmidt; (c) MO-Moscow, AP-Apatity. Vertical arrow marks a moment of main radio onset (1102 UT). Note the prompt impulse-like increase seen by Norilsk, Cape Schmidt and Moscow stations. (d) Asymptotic cones (AC) of acceptance in the system of solar-ecliptic coordinates for a number of neutron monitor stations from Figures 5a–5c and for the Terre Adelie (TA) station. Solid parts of lines denote the portions of maximal response of AC for high-latitude stations (1–3 GV) and for the midlatitude Moscow station (2.4–3.0 GV). The equal pitch angle lines are depicted relative to the derived axis of symmetry direction. An asterisk is derived direction of maximal intensity during the impulse-like increase. By circles with a point and a cross are marked the IMF directions (data of ACE spacecraft) from 1100 to 1200 UT of 28 October 2003.

and latitude, respectively, in the GSE system); a value  $A(R) = 1$  for allowed and 0 for forbidden trajectories, and  $F(\theta(R)) \sim \exp(-\theta^2/C)$  is the pitch angle distribution of RSP with a characteristic parameter  $C$  [Shea and Smart, 1982]. So, there are six parameters of anisotropic solar proton flux outside the magnetosphere ( $\Phi$ ,  $\Lambda$ ,  $J_0$ ,  $\gamma$ ,  $\Delta\gamma$ , and  $C$ ) to be determined by a least squares procedure in a comparison of computed responses with observations. With the count rate data corrected for atmospheric pressure by the two attenuation lengths method [Kaminer, 1968] and modeled NM responses, a system of constrained equations may be arranged and the procedure is reduced then to solving the nonlinear least squares problem:

$$SN = \sum_j \left[ \left( \frac{\Delta N}{N} \right)_j^{calc} - \left( \frac{\Delta N}{N} \right)_j^{observ} \right]^2 \Rightarrow \min. \quad (2)$$

Characteristics of RSP cannot be always described within the framework of a particle flux from one direction. Therefore we used three models of the particle flux: a unidirectional propagation along an anisotropy axis; a bidirectional distribution, specifying the particle flux as superposition of direct and backward fluxes with independent parameters ( $J_0$ ,  $\gamma$ ,  $\Delta\gamma$ ,  $C$ ); and the third model with two completely independent fluxes including independent anisotropy axes. Accordingly, the number of parameters in the second model grows up to 10 and in the third grows up to 12.

[20] In search of an optimization minimum of equation (2), the models are used in the following order: if the optimization error on the unidirectional model does not converge, the model with bidirectional flux is applied. Also, if in this case there is a great residual error, the third model with completely independent particle fluxes is used. With the purpose of verifying and refining the technique under consideration, we used the third model for the events that are consistently described by the unidirectional model. It turns out that in this model of two independent beams the second beam has orders of magnitude lower flux than the first. The final solution is only slightly different from that for the unidirectional model.

## 5.2. Distribution of the Increase Effect Over the Globe

[21] Figures 5a–5c shows the increases in counting rates at several Russian neutron monitor (NM) stations Apatity, Barentsburg (an archipelago Spitsbergen, Arctic), Cape Schmidt, Norilsk, and Moscow in comparison with that at the McMurdo station (Antarctica). The vertical arrow marks the main solar radio onset in the wide range of emissions from microwaves to meter waves (see section 3). The microwave, hard X-ray, and gamma-ray emission show that this is the start of the acceleration of both electrons and protons, and it is plausible to consider the same time interval for the acceleration of relativistic protons. Two important features attract our attention in Figures 5a–5b: (1) the strong north-south (NS) asymmetry in the RSP flux demonstrated by the difference in the GLE excesses at the two sea level stations with the highest northern (Barentsburg) and southern (McMurdo) latitudes (Figure 5a) and (2) the impulse-like increase observed at Norilsk station. This earliest proton arrival has been also detected



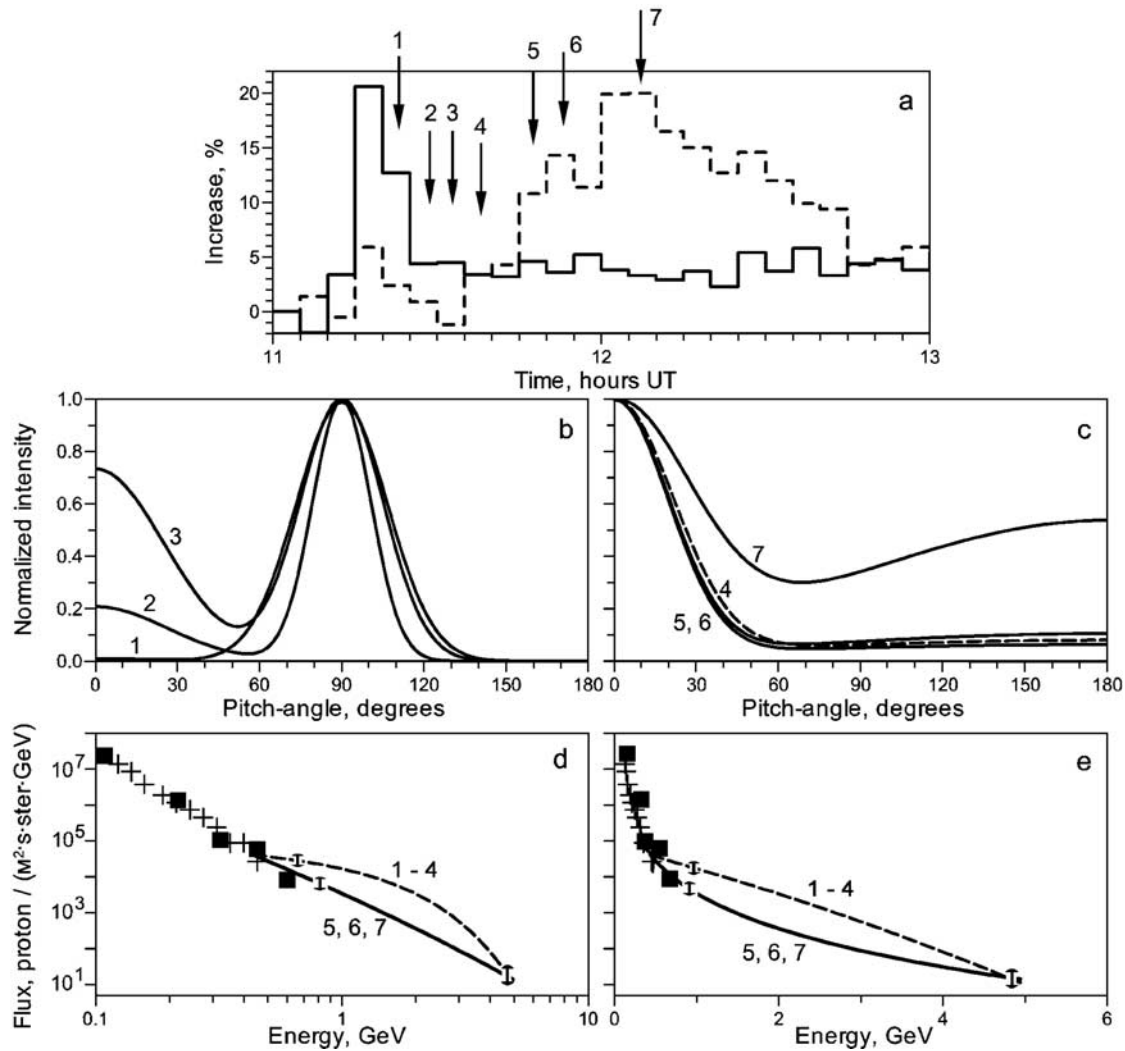


**Figure 6.** Dynamics of relativistic solar protons in the GLE of 28 October 2003: (a) increase profiles at neutron monitor stations Norilsk (solid line) and Cape Schmidt (dashed line). Numbered arrows are the moments of time (Table 2), when parameters of RSP were derived. Dynamics of derived pitch angle distribution: (b) during the initial impulsive increase; (c) during the main intensity maximum. Dynamics of derived energy spectra: (d) in double logarithmic, (e) in semilogarithmic scale. Data of direct solar proton measurements are shown by crosses (balloons) and blacked squares (GOES-10/11 spacecrafts).

at the Cape Schmidt and Moscow stations (Figures 5b–5c). It may be a manifestation of the so-called “prompt component” (PC) of RSP [Vashenyuk and Miroshnichenko, 1998]. On the other hand, the second peak at the profile of Cape Schmidt station (Figure 5b) and the data of Apatity NM (Figure 5c) display the so-called “delayed component” (DC) of RSP. Notice especially that the amplitude of increase at the Moscow station is larger than that at Apatity, in spite of the higher cutoff rigidity of the Moscow station. This is one of the manifestations of the strong anisotropy in the RSP flux.

[22] Figure 5d shows a celestial sphere in the solar-ecliptic (GSE) coordinate system, together with asymptotic cones (AC) of acceptance for different stations in the range of rigidities from atmospheric cutoff  $\sim 1$  GV (430 MeV) to about 10 GV (assumed upper limit in the SCR spectrum). Solid parts of the lines denote the portions of maximal response of AC for high-latitude stations (1–3 GV) and that

for the midlatitude Moscow station (2.4–3.0 GV). A map in Figure 5d also shows the lines of equal pitch angles relative to the derived anisotropy axis at the time of the second GLE maximum at 1200 UT (see Figures 5a–5c), which in the case of adiabatic particle transport must coincide with the IMF direction. The latter was estimated by the ACE data (see section 2) and is shown in Figure 5d by circles with a point (antisunward) and a cross (sunward). As one can see, there is no exact correspondence between the derived anisotropy axis and the IMF direction measured by ACE in the highly nonnominal IMF configuration at the interface between an ICME and a corotating stream. Some uncertainty comes from the fact that the IMF data were obtained by ACE 40 min before the magnetic field structure arrived at the Earth and are valid for our purpose if the IMF did not vary significantly during the 40-min transportation with the solar wind ( $\sim 700$  km/s) from the spacecraft to the Earth. One also needs to take into account the limited accuracy of

**Table 2.** Energy Spectra, Pitch Angle Distributions, and Apparent Viewing Directions of Relativistic Solar Protons

	Time, UT	Source 1						Source 2					
		$\gamma_1$	$\Delta\gamma_1$	C1	$\theta_1$	$\Phi_1$	$J_{10}$	$\gamma_2$	$\Delta\gamma_2$	C2	$\theta_2$	$\Phi_2$	$J_{20}$
1	1125	0.63	0.16	0.40	−57	260	80	2.2	0.31	0.17	1	135	7900
2	1130	1.15	0.24	0.42	−61	253	920	1.2	0.6	0.17	−2	144	4400
3	1135	2.0	0.16	0.40	−60	255	2200	1.2	0.7	0.15	−5	144	3000
4	1140	0.84	0.91	0.28	−60	256	2970	0.8	0.2	10.27	60	76	247
5	1150	4.39	0.0	0.24	−59	253	33100	1.5	0.42	7.41	59	73	3600
6	1155	3.93	0.0	0.23	−63	260	22200	0.72	0.38	11.82	63	80	1450
7	1210	4.38	0.0	0.44	−62	235	56400	5.60	0.01	5.36	62	55	33300

determination of the anisotropy axis ( $\pm 10^\circ$ ). Besides, we considered 30-min averages of the IMF vector only because relativistic solar protons do not feel fast changes in the IMF and are governed by it only on the scales comparable with their gyroradii. Since a maximum SCR flux has been noted by the stations McMurdo, Cape Schmidt, and Terre Adélie (not shown in Figures 5a–5c), the direct flux of relativistic solar protons seemed to arrive from south of the ecliptic plane along the IMF, which was inclined to the ecliptic plane. On the other hand, some stations that accepted radiation from the opposite direction (for example, Apatity and Barentsburg), as well as the stations accepted the particles with large pitch angles, have registered a small increase delayed by about 15 min relative to the direct flux.

[23] An unusual feature in this case also was that the maximum intensity of the PC has been observed by the Norilsk NM, which accepted the incoming radiation from the direction nearly perpendicular to the IMF. An asterisk in Figure 5d shows the symmetry axis of PC flux obtained by the quantitative analysis (section 5.2). This analysis also shows that the prompt increase of the Moscow NM profile (Figure 5c) was caused by particles arriving from the same directions as at Norilsk station (note the overlapping portion of their asymptotic cones in Figure 5d). At the same time, the symmetry axis of the direct DC flux is close to the estimated direction of the IMF (Figure 5d).

### 5.3. Derived Parameters of Solar Proton Flux

[24] Figure 6 and Table 2 show the RSP parameter dynamics in the course of this GLE. Intensity-time profiles at the stations Norilsk and Cape Schmidt at the specified instants 1–7 of model calculations are plotted in Figure 6a. Dynamical changes of the pitch angle distribution (PAD) of the prompt component (PC) of RSP (initial pulse of intensity) are demonstrated in Figure 6b (instants 1–3). The peculiarity here is that the maximum intensity of PC was due to the particle flux from a direction nearly perpendicular to the mean IMF and to the symmetry axis of RSP (this direction is indicated by an asterisk in Figure 5d). Also, Figure 6c shows the PAD evolution during the main intensity increase dominated by the delayed component (instants 5–7). Such behavior can be explained by a strong deflection of an anisotropic bunch of relativistic solar protons on a kink of the IMF existing on the way of the bunch to the Earth (section 7). As seen from the data of Table 2 and Figures 5d and 6c, in the beginning of the main increase (instants 5 and 6) all particles arrived already approximately along the IMF but from the antisunward direction. Near the peak of the main increase (instant 7) the PAD becomes broader and additional flux from the

opposite direction has caused a bidirectional anisotropy. The dynamics of derived spectra are shown in double logarithmic (d) and semilogarithmic (e) scales. Spectra derived for instants 1–4 obviously correspond to the prompt component (PC) and are approximated by a dashed curve in Figures 6d and 6e. Spectra derived for instants 5–7 correspond to the delayed component (DC) of RSP. We note that within the estimated error limits the spectrum of PC can be approximated by an exponential in energy:  $J = 1.5 \times 10^5 \exp(-E/0.4) \text{ m}^{-2} \text{ s}^{-1} \text{ st}^{-1} \text{ MeV}^{-1}$ . During the maximum of the main increase (instants 5–7) the spectrum becomes a power law in energy: It can be approximated by a power law:  $J = 3.5 \times 10^3 E^{-3.5} \text{ m}^{-2} \text{ s}^{-1} \text{ st}^{-1} \text{ MeV}^{-1}$  [Vashenyuk *et al.*, 2005]. The lower limit of the spectra derived from the ground based neutron monitor data is 450 MeV (atmospheric cutoff). The direct solar proton measurements in adjacent energy ranges (100–700 MeV) show good agreement with the derived RSP spectra. By crosses in Figures 6d–6e are shown the data of balloon flights over Apatity (joint experiment of Lebedev Physical Institute and Polar Geophysical Institute) [Bazilevskaya and Svirzhevskaya, 1998]. Black squares are derived intensities from the differential proton channels at GOES-10/11 spacecraft (<http://sec.noaa.gov/ftpmenu/lists/pchan.html>). It is seen that the spectrum of direct solar protons is an extension with the same slope of the derived spectrum up to 100 MeV.

[25] The above analysis gives some evidence that the RSP flux obtained by the optimization methods in the event of 28 October 2003 displays two populations (components) of relativistic particles. A prompt component (PC), with the hard energy spectrum of exponential type and strong anisotropy, manifested itself in the form of an impulse-like increase at several NM stations. A slow, or delayed, component (DC) has a softer energy spectrum in the power law form and displays first field-aligned streaming from the antisunward direction and then a reverse flux causing bidirectional anisotropy. Below we discuss several possible ways to incorporate all observational data and derived parameters of accelerated particles in a general consistent scenario of the event under study.

### 6. Energetic Electrons and Protons

[26] In Figure 7 the increase profiles of solar electrons and protons in different energy ranges are shown in comparison with enhancements registered by neutron monitors McMurdo and Norilsk. Note an impulsive increase (1120–1140 UT) seen for subrelativistic 38–53 keV electrons and relativistic protons (neutron monitors). The gradual late increase is observed for protons of moderate energies and

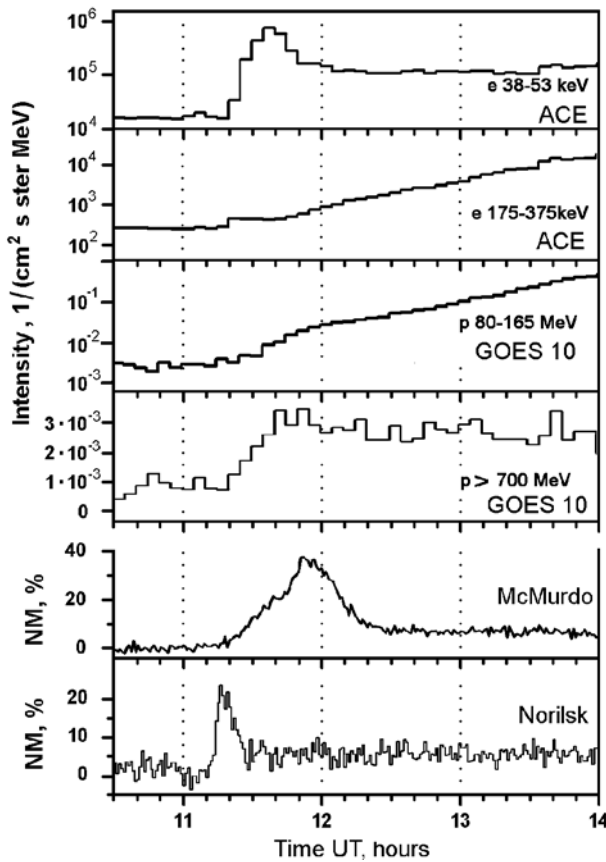


**Figure 7.** Increase profiles of solar electrons and protons in different energy ranges. From up to bottom: electrons 38–53 KeV and 175–315 as measured on ACE spacecraft, protons 80–165 and 510–700 MeV (GOES 11 data), neutron monitors McMurdo and Norilsk. Note an impulsive increase seen in the low-energy electron channel.

relativistic electrons (175–375 keV). The time-intensity profile of protons >700 MeV, measured on GOES-10, represents apparently a superposition of the impulselike increase of relativistic solar protons and a more gradual rise of protons with energy of several hundreds of MeV. It is necessary to specify that as mentioned earlier, the prompt and delayed components of RSP are connected to active processes in a solar corona having the temporary scale not exceeding several tens of minutes. A gradual intensity rise cannot be related to coronal active processes and rather is reflection of coronal transport and accumulation in the closed magnetic structures of corona and interplanetary space. The impulsive increase on the other hand should be directly connected to the prompt arrival of particles after an impulsive injection. From the arrival times of particles of various species and energies it is possible to estimate the release time on the Sun and the path length traveled by particles in interplanetary space. In Table 3 the onset times of protons from data of neutron monitors, the GOES-10 and 11 spacecraft (<http://sec.noaa.gov/ftpmenu/lists/pchan.html>), as well as reciprocal values ( $1/\beta$ ) of particle speed in units of the speed of light are presented. The values of  $1/\beta$  are given for the average energy of each detector channel. In the GOES data only the high-energy proton channels were

used, as the data of proton energies lower than 100 MeV were contaminated by the higher-energy particles [Smart and Shea, 1999].

[27] In Figure 8 the arrival time at the Earth of protons of various energies is plotted versus the reciprocal of their speed. For protons with energy higher than 100 MeV the traveled path is equal to 2.2 AU if we choose the release time at the Sun near 1055 UT (=1103 UT – 8 min). In Figure 8 we put also the point corresponding to the average speed of the electrons 8.5 KeV responsible for the type III radio emission detected by the Wind/WAVES instrument (section 3) and their traveled path of 1.04 AU. Electron measurements by the Wind and ACE spacecraft are discussed elsewhere in this issue [Klassen *et al.*, 2005; Simnett, 2005]. From the energy dispersion of arrival times at Wind, Klassen *et al.* derive a solar release time of 1105 UT (=1113 UT – 8 min) for the onset of the impulsive electron flux increase observed up to about 180 keV between 1120 and 1140 UT (Figure 7). The energy dispersion of the onset times and of the times of maxima imply an interplanetary path length similar to the nominal Parker spiral length (up to 1.1 AU), and exclude a path length comparable to that of the protons (S. Krucker, personal communication, 2005).

## 7. Discussion and Conclusions

[28] Different particle populations were detected at the Earth during the GLE of 28 October 2003, which was associated with a flare east of central meridian. This event is a further case that was a priori not well-connected with the Earth in the usual picture of the interplanetary magnetic structure. The very early GLE signature observed at Tsumeb near the subsolar point is tentatively attributed to the arrival of relativistic neutrons from the Sun, similar to findings by Bieber *et al.* [2005] for the 28 October 2003 GLE and, e.g., by Debrunner *et al.* [1997] for that of 24 May 1990. A few minutes later, primary relativistic protons reach the Earth, as demonstrated by the GLE detection on the nightside. The evidence for neutrons might support the interpretation that the subsequent protons are actually produced by the decay of primary neutrons on the well-connected interplanetary magnetic field line, as proposed for the similarly poorly

**Table 3.** Onset Times for the Particle Event October 28 2003

Ep or Ee, MeV	$\Delta E$ , MeV	$1/\beta_{Av}$	Time
Protons			
<i>Neutron Monitor</i>			
1000	430–9000	1.14	11:12 $\pm$ 1
<i>GOES-10</i>			
130	80–165	2.09	11:32 $\pm$ 2
320	165–500	1.51	11:25 $\pm$ 5
380	350–420	1.42	11:20 $\pm$ 5
470	420–510	1.34	11:20 $\pm$ 5
750	>700	1.20	11:18 $\pm$ 2
<i>GOES-11</i>			
130	80–165	2.09	11:28 $\pm$ 2
320	165–500	1.51	11:25 $\pm$ 5
Electrons			
<i>Wind/WAVES</i>			
8.5	5–20	5.55	11:43 $\pm$ 1

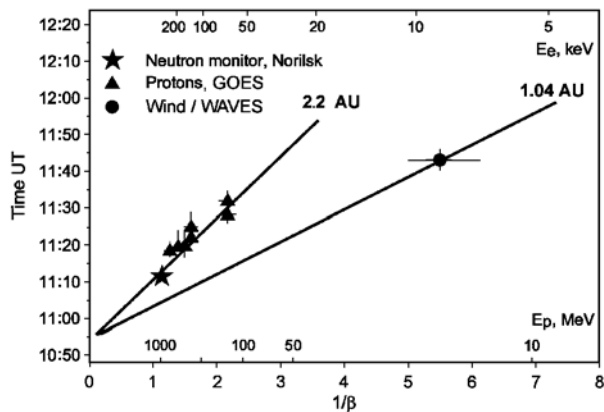


**Figure 8.** Plot of proton and electron arrival time versus reciprocal particle speed in units of speed of light. The lines correspond to best fits of traveled interplanetary paths for two groups of particles: 1.1 AU for subrelativistic electrons and 2.2 AU for high energy solar protons and relativistic electrons. As the release time the onset of the most conspicuous electromagnetic emissions from the corona 1054 UT has been chosen.

connected GLE on 19 October 1989 [Shea *et al.*, 1991]. However, the observation that neutrons, provided our interpretation of the Tsumeb signal is correct, occurred several minutes before the release of protons, argues against this interpretation.

[29] We summarize the observations of energetic charged particles as follows:

[30] 1. The initial release time of the high-energy protons corresponds to the onset of the most conspicuous electromagnetic emissions from the corona (1102–1103 UT, as seen from the Earth), and to a travel distance slightly above 2 AU in interplanetary space.

[31] 2. The simultaneous acceleration of electrons at energies near 10 keV and their escape to the Wind spacecraft is fully confirmed by the radio observations, which point to acceleration sites near the footpoint of the nominal Parker spiral, at several tens of heliocentric degrees from the flare site (section 3).

[32] 3. Although electrons up to 180 keV travel along a similar interplanetary path as the 10 keV electrons, they seem to be released about 10 min later. Again, potential acceleration sites can be identified in the meter wave imaging data (see discussion below).

[33] 4. For protons of relativistic energies the traveled path appears to be twice as large as the nominal Parker spiral. These particles, as is argued below, could come to the Earth directly from the flare on the eastern part of the solar disk along the loop-like IMF structure formed by an ICME from preceding activity on the Sun. It cannot be excluded that relativistic electrons (energy above 170 keV) propagated to the Earth along the same way as high-energy protons. In this case the delay in arrival of relativistic electrons could be explained by the longer path along the loop-like structure of IMF.

[34] Figure 9a shows the structure of interplanetary medium between the Sun and Earth during the event on 28 October 2003 suggested on the basis of the IMF,

solar wind, and energetic solar particle data. Early this day the shock driven by an ICME from the X1.2/3B flare on 26 October, 0617 UT in active region AR10486 has arrived at the Earth. The Earth remained inside the ICME from approximately 0200 UT till 0840 UT, when a corotating high-speed solar wind stream (CS) started (Figure 1). The

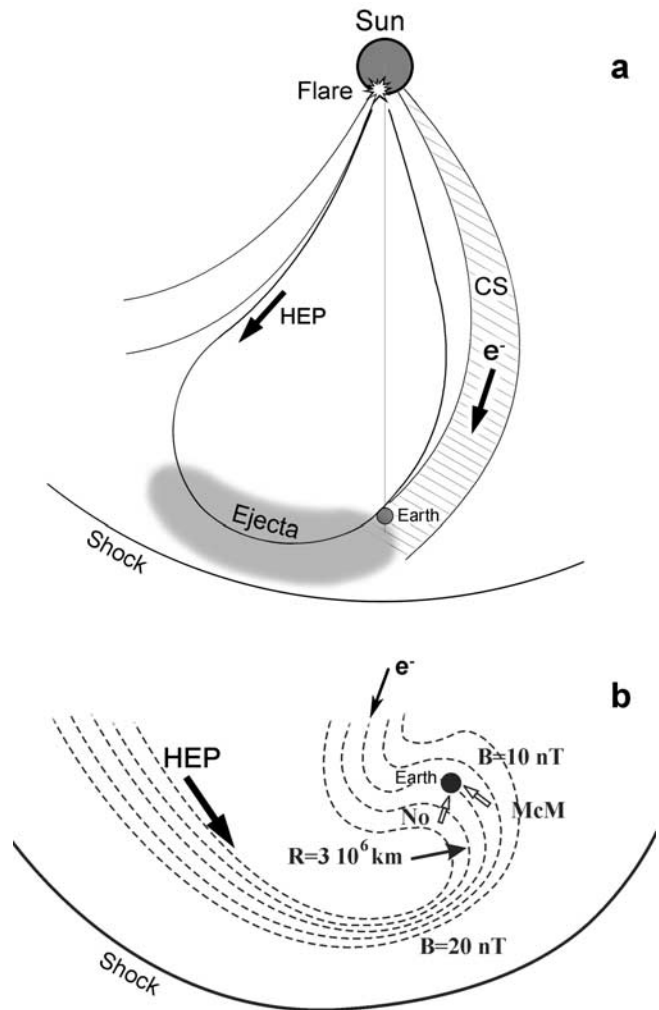


**Figure 9.** (a) Sketch of the proposed model for the IMF structure during the 28 October, 2003 SPE. The Earth is at a boundary area between an ejecta from the flare 26 October and the corotating stream (CS) commenced to Earth shortly before the event. By means of looped IMF structure inside ejecta, the Earth is connected to a flare site in eastern part of solar disc. High-energy solar protons (HEP) come to the Earth from antisunward direction. At the same time, the subrelativistic electrons can arrive to the Earth from a source in western part of solar disk along of a Parker spiral IMF line, connected with a corotating stream. (b) The spatial structure of IMF near the Earth during the 28 October 2003 GLE, reconstructed with use of IMF and solar wind data. The dotted lines are the IMF field lines and arrows are average directions of relativistic proton flux registered by neutron monitors in McMurdo (McM) and Norilsk (No). By essential detail here is the sharp kink of a magnetic field with the radius of curvature  $3 \times 10^6$  km comparable with Larmor radii of relativistic solar protons.



source of the stream seems to be a coronal hole in the northwestern solar quadrant, northwest of AR10486. The situation shown in Figures 1 and 9a, where an ICME is followed by a corotating solar wind stream, is not unusual and is observed approximately in 30% of magnetic cloud-type ICMEs [Burlaga *et al.*, 1998]. Thus in the beginning of the event the Earth was in a boundary area between the ICME and the corotating stream. If the ICME includes a loop or flux rope rooted in the corona, this scheme can explain the arrival of high-energy protons (HEP) from the antisunward direction. A similar scheme of fast arrival of particles from eastern flares was considered by Richardson *et al.* [1991] and Richardson and Cane [1996], while Torsti *et al.* [2004] discussed another large particle event inside a magnetic cloud. In the scheme shown in Figure 9a the low-energy electrons released from the western part of the solar disc and traced by the type III radio emission also can reach the Earth along the Parker spiral IMF lines related to the corotating stream. It is interesting to note (Figure 3) that some metric radio sources at the time of the DH type III bursts are indeed located near the coronal hole.

[35] Figure 9b shows the spatial structure of the IMF near the Earth during the 28 October 2003 GLE, reconstructed with use of IMF and solar wind data measured on the ACE spacecraft for several hours before and after beginning of the GLE (see Figure 1). The dotted lines show the IMF field lines and arrows are average directions of RSP fluxes registered by neutron monitors in McMurdo and Norilsk. An essential detail here is the sharp kink of the magnetic field. Its radius of curvature inferred from the observed solar wind speed and variation of the magnetic field vector in Figure 1 ( $3 \times 10^6$  km) was comparable with Larmor radii of protons with rigidities 1–3 GV, giving the main contribution to the count rate of neutron monitors. We carried out trajectory computations in the magnetic structure shown in Figure 9b, which allowed us to understand the unusual behavior of the relativistic proton anisotropy (Figure 6). Since the bunch of relativistic protons of the prompt component had small pitch angles, it strongly deviated at the IMF kink. The particles with great pitch angles are scattered a little on the kink and pass through it keeping the direction of movement along the magnetic field. This can explain the observed effect, namely that the strongly anisotropic particle bunch of prompt solar protons that was registered by neutron monitor stations at Norilsk and Moscow (Figure 5) turned into the direction almost perpendicular to the IMF. The delayed component particles, the majority having large pitch angles, scattered a little on the kink of the IMF. So the McMurdo station looking along the IMF registered a delayed RSP, coming along the IMF from the antisunward direction. Thus both prompt and delayed components of relativistic solar protons came from the antisunward direction. Given the longer path in interplanetary space, their arrival time is consistent with acceleration during the brightest electromagnetic emissions of the flare, and their arrival direction is consistent with acceleration near the flare site located east of the central meridian. As the prompt and delayed relativistic solar protons propagated under identical conditions in interplanetary space, the observable difference in spectra and pitch angle distributions should be solely due to the processes of generation and release from the solar corona. Our estimations show

also that the effects of interplanetary propagation influence a little the spectral form of relativistic solar protons, at least for the prompt component of RSP.

[36] It is not entirely clear how the electrons detected at ACE and Wind fit within the scenario (see Klassen *et al.* [2005] and Simnett [2005] for other attempts of interpretation). The first impulsive electrons at energies (30–180) keV detected by both spacecraft (1120–1140 UT in the top panel of Figure 7) are clearly released later at the Sun than the 10 keV electrons emitting the bright DH type III burst, which seem to be accelerated in the western hemisphere. However, like the 10 keV electrons, they have a short interplanetary travel distance, much shorter than the 2 AU traveled by the high-energy protons. Long-lasting electron acceleration near the foot of the well-connected nominal Parker spiral is shown by the metric radio sources. This region may be a candidate source for the escaping impulsive electrons, too.

[37] If relativistic protons reach the Earth along loop-shaped IMF lines from AR 10486 east of the central meridian, one expects to see energetic electrons, too, since hard X-ray and nuclear gamma-ray emission occur at about the same time. Electrons with speed between 0.5 times the speed of light and the speed of light, released at the onset of this emission (1102 UT) onto a field line of length 2 AU are expected to arrive at the Earth between 1111 UT and 1127 UT. These arrival times are not inconsistent with the slowly rising high-energy flux observed at ACE and Wind after the initial impulsive peak (cf. Figure 7, second panel from top). The timing thus indicates a possible common origin of relativistic electrons and relativistic protons in the flaring AR 10486. A more detailed analysis is necessary, however, since the long rise and the weakly anisotropic electron distribution [Simnett, 2005] suggest that the electrons do not freely stream out of the corona and along the IMF.

[38] **Acknowledgments.** The authors acknowledge the principal investigator teams of the worldwide network of neutron monitors, especially those at Bartol Research Institute (NSF grant ATM 0000315) and P. Stoker (Tsumeb and Potchefstroom) for making 1 min data available, M. Storini, IFSI, Roma (Roma and LARC), V.G. Yanke and E.A. Eroshenko from IZMIRAN Cosmic Ray Group, Moscow. They are grateful to the PI teams of the WAVES and SWE instruments aboard the Wind spacecraft, R. Gold of JHU Applied Physics Laboratory for the data of the EPAM instrument onboard of ACE spacecraft, and of EIT aboard SOHO for making their data available via their web-pages, to the Solar Data Analysis Center at the Goddard Space Flight Center (GOES data), and to the National Geophysical Data Center at NOAA (RSTN data). A. Klassen, A. Lecacheux, and X. Moussas are thanked for providing radio spectra from the Potsdam-Tremsdorf, Nançay (Decameter Array) and Thermopylae Observatories, and the referees for their careful reading of the manuscript. The Russian coauthors of this paper acknowledge the Russian Foundation of Basic Research for financial support (RFBR projects 02-02-16987, 02-02-39032, 03-02-96026 and 04-02-26806). The neutron monitor at Terre Adélie is operated by the Institute Paul-Emile Victor (IPEV) and Paris Observatory/LESIA. The Nançay Radio Observatory is funded by the French Ministry of Education, the CNRS, and the Région Centre. KLK is grateful to E. Flueckiger and his group for helpful discussions.

[39] Arthur Richmond thanks Sergey Kuznetsov and another reviewer for their assistance in evaluating this paper.

## References

- Bazilevskaya, G. A., and A. K. Svirzhevskaya (1998), On the stratospheric measurements of cosmic rays, *Space Sci. Rev.*, **85**, 431–521.
- Bieber, J. W., J. Clem, P. Evenson, and R. Pyle (2005), Relativistic solar neutrons and protons on 28 October 2003, *Geophys. Res. Lett.*, **32**, L03S02, doi:10.1029/2004GL021492.
- Bougeret, J.-L., et al. (1995), WAVES: The Radio and Plasma Wave investigation on the Wind spacecraft, *Space Sci. Rev.*, **71**, 231–263.

- Burlaga, L., et al. (1998), A magnetic cloud containing prominence material: January 1997, *J. Geophys. Res.*, **103**, 277–285.
- Cane, H. (2000), Coronal mass ejections and Forbush decreases, *Space Sci. Rev.*, **93**, 55–77.
- Cramp, L. J., M. L. Duldig, E. O. Flueckiger, J. E. Humble, M. A. Shea, and D. F. Smart (1997), The October 22, 1989 solar cosmic ray enhancement: An analysis of the anisotropy and spectral characteristics, *J. Geophys. Res.*, **102**, 24,237–24,248.
- Debrunner, H., E. O. Flueckiger, and P. Stein (1990), On the sensitivity of a NM-64 standard neutron monitor at sea level to solar neutrons in dependence of the angular distance of the station from the sub-solar point, *Proc. Int. Cosmic Ray Conf. 21st*, **5**, 129–132.
- Debrunner, H., et al. (1997), Energetic neutrons, protons, and gamma rays during the 1990 may 24 solar cosmic-ray event, *Astrophys. J.*, **479**, 997–1011.
- Delaboudinière, J. P., et al. (1995), EIT: Extreme ultraviolet imaging telescope for the SOHO mission, *Solar Phys.*, **162**, 291–312.
- Evenson, P., P. Meyer, and K. R. Pyle (1983), Protons from the decay of solar flare neutrons, *Astrophys. J.*, **274**, 875–882.
- Gros, M., et al. (2004), INTEGRAL/SPI observations of the 2003 Oct 28 solar flare, in *Proc. 5th INTEGRAL Science Workshop, ESA Spec. Publ. 552*, pp. 669–676, Eur. Space Agency, Paris.
- Ivanov, K. G., A. F. Kharshiladze, and E. P. Romashets (2005), Solar-terrestrial storms in October 2003. 1. Solar sources and interplanetary disturbances near Earth, *Geomagn. Aeron.*, **45**, 5–22.
- Kahler, S. W., and D. V. Reames (1991), Probing the magnetic topologies of magnetic clouds by means of solar energetic particles, *J. Geophys. Res.*, **96**, 9419–9424.
- Kaminer, N. S. (1968), On account of barometrical effect of the neutron component during solar proton flares, *Geomagn. Aeron.*, **8**, 806.
- Kerdraon, A., and J. Delouis (1997), The Nancy Radioheliograph, in *Coronal Physics from Radio and Space Observations, Lecture Notes in Phys.*, vol. 483, edited by G. Trottet, pp. 192–201, Springer, New York.
- Klassen, A., et al. (2005), Solar energetic electrons related to the 28 October 2003 flare, *J. Geophys. Res.*, **110**, A09S04, doi:10.1029/2004JA010910.
- Klein, K.-L., E. L. Chupp, G. Trottet, A. Magun, P. P. Dunphy, E. Rieger, and S. Urpo (1999), Flare-associated energetic particles in the corona and at 1 AU, *Astron. Astrophys.*, **348**, 271–285.
- Klein, K.-L., G. Trottet, P. Lantos, and J.-P. Delaboudinière (2001), Coronal electron acceleration and relativistic proton production during the 14 July 2000 flare and CME, *Astron. Astrophys.*, **373**, 1073–1082.
- Kuznetsov, S. N., I. N. Myagkova, V. G. Kurt, B. Y. Yushkov, and K. Kudela (2005), High energy neutral emissions observed by the SONG experiment onboard CORONAS during some of the large October–November solar flares, *Adv. Space Res.*, in press.
- Lecacheux, A. (2000), The Nancy Decameter Array: A useful step towards giant new generation radio telescopes for long wavelength radio astronomy, in *Radio Astronomy at Long Wavelengths, Geophys. Monogr. Ser.*, vol. 119, edited by R. Stone et al., pp. 321–328, AGU, Washington, D. C.
- Lockwood, J. A., H. Debrunner, and E. O. Flueckiger (1990), Indications for diffusive coronal shock acceleration of protons in selected solar cosmic ray events, *J. Geophys. Res.*, **95**, 4187–4201.
- Lüthi, T., A. Lüdi, and A. Magun (2004), Determination of the location and effective angular size of solar flares with a 210 GHz multibeam radiometer, *Astron. Astrophys.*, **420**, 361–370.
- Miroshnichenko, L. I., K.-L. Klein, G. Trottet, P. Lantos, E. V. Vashenyuk, and Y. V. Balabin (2004), Electron acceleration and relativistic nucleon production in the 2003 October 28 solar event, paper presented at 35th COSPAR Scientific Assembly, Comm. on Space Res., Paris.
- Miroshnichenko, L. I., K.-L. Klein, G. Trottet, P. Lantos, E. V. Vashenyuk, and Y. V. Balabin (2005), Electron acceleration and relativistic nucleon production in the 2003 October 28 solar event, *Adv. Space Res.*, in press.
- Ogilvie, K. W., et al. (1995), SWE: A comprehensive plasma instrument for the Wind spacecraft, *Space Sci. Rev.*, **71**, 55–77.
- Richardson, I. G., and H. V. Cane (1996), Particle flows observed in ejecta during solar event onsets and their implication for the magnetic field topology, *J. Geophys. Res.*, **101**, 27,521–27,532.
- Richardson, I. G., H. V. Cane, and T. T. von Rosenvinge (1991), Prompt arrival of solar energetic particles from far eastern events: The role of large-scale interplanetary magnetic field structure, *J. Geophys. Res.*, **96**, 7853–7860.
- Shea, M. A., and D. F. Smart (1982), Possible evidence for a rigidity-dependent release of relativistic protons from the solar corona, *Space Sci. Rev.*, **32**, 251–271.
- Shea, M. A., D. Smart, M. Wilson, and E. Flueckiger (1991), Possible ground level measurements of solar neutron decay protons during the 19 October 1989 solar cosmic ray event, *Geophys. Res. Lett.*, **18**, 829–832.
- Simnett, G. (2005), Near relativistic electron emission following the 28 October 2003 X 17 flare, *J. Geophys. Res.*, **110**, A09S01, doi:10.1029/2004JA010789.
- Skoug, R. M., J. T. Gosling, J. T. Steinberg, D. J. McComas, C. W. Smith, N. F. Ness, Q. Hu, and L. F. Burlaga (2004), Extremely high speed solar wind: 29–30 October 2003, *J. Geophys. Res.*, **109**, A09102, doi:10.1029/2004JA010494.
- Smart, D. F., and M. A. Shea (1999), Comment on the use of GOES solar proton data and spectra in solar proton dose calculations, *Radiat. Meas.*, **30**, 327–335.
- Stoker, P. H., and M. Lemmer (1992), The sensitivity of the Tsumeb neutron monitors to solar event neutrons, *Proc. 22nd Int. Cosmic Ray Conf.*, **3**, 33–36.
- Torsti, J., E. Riihonen, and L. Kocharov (2004), The 1998 May 2–3 magnetic cloud: An interplanetary “highway” for solar energetic particles observed with SOHO/ERNE, *Astrophys. J.*, **531**, L75–L77.
- Tsyganenko, N. A. (2002a), A model of the near magnetosphere with a down-dusk asymmetry: 1. Mathematical structure, *J. Geophys. Res.*, **107**(A8), 1179, doi:10.1029/2001JA000219.
- Tsyganenko, N. A. (2002b), A model of the near magnetosphere with a down-dusk asymmetry: 2. Parametrization and fitting to observations, *J. Geophys. Res.*, **107**(A8), 1176, doi:10.1029/2001JA000220.
- Vashenyuk, E. V., and L. I. Miroshnichenko (1998), Characteristics of generation and transport of solar protons during the event of September 29, 1989, *Geomagn. Aeron.*, **38**, 129–135.
- Vashenyuk, E. V., O. V. Mingalev, and B. B. Gvozdevsky (2003a), Dynamics of the spectra and the problem of relativistic solar proton generation: Model investigations (in Russian), *Izv. RAN Phys. Ser.*, **67**, 455–458.
- Vashenyuk, E. V., Y. V. Balabin, and B. B. Gvozdevsky (2003b), Relativistic solar proton dynamics in large GLE of 23rd solar cycle, *Proc. Int. Cosmic Ray Conf. 28th*, **6**, 3401–3404.
- Vashenyuk, E. V., Y. V. Balabin, J. Perez-Peraza, A. Gallegos-Cruz, and L. Miroshnichenko (2005), Some features of the sources of relativistic particles at the Sun in the solar cycles 21–23, *Adv. Space Res.*, in press.
- Veselovsky, I., et al. (2004), Solar and heliospheric phenomena in October–November 2003, Causes and effects, *Space Res.*, **42**, 453–508.
- Yashiro, S., N. Gopalswamy, G. Michalek, O. C. St. Cyr, S. P. Plunkett, N. B. Rich, and R. A. Howard (2004), A catalog of white light coronal mass ejections observed by the SOHO spacecraft, *J. Geophys. Res.*, **109**, A07105, doi:10.1029/2003JA010282.

Y. V. Balabin, B. B. Gvozdevsky, and E. V. Vashenyuk, Polar Geophysical Institute, Apatity, Murmansk Region, 184209, Russia. (vashenyuk@pgi.kolasc.net.ru)

K.-L. Klein, P. Lantos, and G. Trottet, Observatoire de Paris, LESIA, CNRS-UMR 8609, F-92195 Meudon, France.

L. I. Miroshnichenko, Pushkov Institute of Terrestrial Magnetism, Ionosphere, and Radio Wave Propagation (IZMIRAN), Troitsk, Moscow Region, 142190, Russia.